Inorganic Chemistry

Article

pubs.acs.org/IC

Effects of Fluorination on Iridium(III) Complex Phosphorescence: Magnetic Circular Dichroism and Relativistic Time-Dependent Density Functional Theory

A. R. G. Smith,[†,‡] M. J. Riley,[‡] P. L. Burn,*[,†,‡] I. R. Gentle,[†,‡] S.-C. Lo,[†,‡] and B. J. Powell*[,†,§]

[†]Centre for Organic Photonics & Electronics, [‡]School of Chemistry & Molecular Biosciences, and [§]School of Mathematics & Physics, The University of Queensland, Brisbane, Queensland 4072, Australia

Supporting Information

ABSTRACT: We use a combination of low temperature, high field magnetic circular dichroism, absorption, and emission spectroscopy with relativistic time-dependent density functional calculations to reveal a subtle interplay between the effects of chemical substitution and spin−orbit coupling (SOC) in a family of iridium(III) complexes. Fluorination at the *ortho* and *para* positions of the phenyl group of *fac*-tris(1-methyl-5-phenyl-3-*n*-propyl-[1,2,4]triazolyl)iridium(III) cause changes that are independent of whether the other position is fluorinated or protonated. This is demonstrated by a simple linear relationship found for a range of measured and calculated properties of these complexes. Further, we show that the phosphorescent radiative rate, k_r, is determined by the degree to which SOC is able to hybridize T_1 to S_3 and that k_r is proportional to the inverse fourth power of the energy gap between these excitations. We show that fluorination in the *para* position leads to a much larger increase of the energy gap than fluorination at the *ortho* position. Theory is used to trace this back to the fact that fluorination at the *para* position increases the difference in electron density between the phenyl and triazolyl groups, which distorts the complex further from octahedral symmetry, and increases the energy separation between the highest occupied molecular orbital (HOMO) and the HOMO-1. This provides a new design criterion for phosphorescent iridium(III) complexes for organic optoelectronic applications. In contrast, the nonradiative rate is greatly enhanced by fluorination at the *ortho* position. This may be connected to a significant redistribution of spectral weight. We also show that the lowest energy excitation, 1A, has almost no oscillator strength; therefore, the second lowest excitation, 2E, is the dominant emissive state at room temperature. Nevertheless the mirror image rule between absorption and emission is obeyed, as 2E is responsible for both absorption and emission at all but very low (<10 K) temperatures.

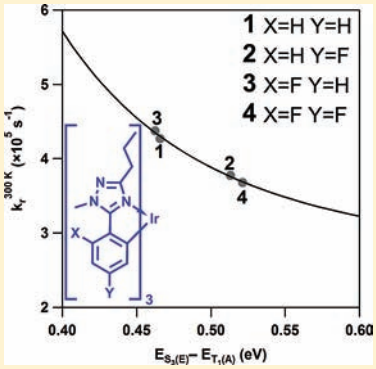

INTRODUCTION

Organic light emitting diodes (OLEDs) based on phosphorescent emitters can efficiently harvest both singlet and triplet excitations.[1−3] From a device point of view this is advantageous, since the internal quantum efficiency can approach 100%,[4] making phosphorescent materials prime candidates for full-color displays[1,5] and solid-state lighting.[6−8]

To date, the best phosphorescent materials for OLEDs are based on iridium(III) complexes.[3,9−11] Ligand modification has been used to tune the emission color,[12] but it is not possible to predict the photoluminescence quantum yields (PLQYs) of the resultant metal complexes.[10,13] The subtle effect played by spin−orbit coupling (SOC), which enables phosphorescence, has been inadequately studied, which makes it difficult to understand the relationship between ligand substitution and the radiative rate of phosphorescence.

For display and lighting applications, the development of highly efficient deep blue OLEDs remains an outstanding problem.[1] Here we focus on *fac*-tris(1-methyl-5-phenyl-3-*n*-propyl-[1,2,4]triazolyl)iridium(III) [Ir(ptz)$_3$; **1**; Figure 1], which displays sky blue phosphorescence with a high PLQY of 66%.[10] Fluorination at the X and/or Y positions (*ortho* and *para* to the triazolyl ring) successfully drives the phosphorescence to a deeper blue (shorter wavelength); however, this also results in a dramatic drop in the PLQY (see Table 1).[10]

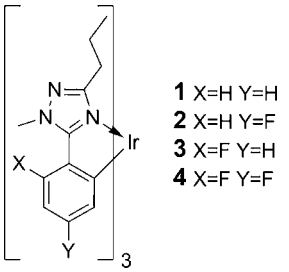

Figure 1. Structures of complexes **1**−**4** investigated in this study based on the parent *fac*-tris(1-methyl-5-phenyl-3-*n*-propyl-[1,2,4]triazolyl)-iridium(III). Fluorination on the ligand phenyl ring blue shifts the emission, but results in a decrease in the PLQY.[10]

Received: August 31, 2011
Published: February 16, 2012

Table 1. Selected Room Temperature Spectroscopic Properties of Iridium(III) Complexes 1−4[a]

	experimental						calculated	
complex	PL λ_{max} (nm)	CIE (x, y)	Φ_{PL}	τ (μs)	k_r ($\times 10^5$ s^{-1})	k_{nr} ($\times 10^5$ s^{-1})	k_r ($\times 10^5$ s^{-1})	ZFS T_1(A) $\Delta E_{1A\text{-}2E}$ (meV)
1	449	0.158, 0.202	0.66 ± 0.07	1.08 ± 0.03	6.1 ± 0.8	3.1 ± 1.0	4.3	11.6
2	428	0.157, 0.127	0.27 ± 0.05	1.25 ± 0.30	2.2 ± 0.9	5.8 ± 2.8	3.8	8.7
3	443	0.155, 0.161	0.06	0.15	4.0	63	4.4	11.3
4	425	0.159, 0.117	0.03 ± 0.01	0.15 ± 0.07	2.0 ± 1.6	65 ± 33	3.7	7.3

[a]Fluorine substitution shifts the emission from sky to deep blue [as evidenced by both the wavelength of the photoluminescence maximim (PL λ_{max}) and the Commission Internationale de l'Eclairage (CIE) coordinates]; however, the PLQY (Φ_{PL}) falls off precipitously. Both the absolute values and the trend in the calculated radiative rates are similar to those determined experimentally. Like the experimental data,[10] complexes **1** and **3** have higher calculated radiative rates than **2** and **4**. Errors have not been reported for complex **3**. Nevertheless it is important to note that the radiative rates of complexes **2** and **4** are the same within experimental error and if there is a difference between the radiative rates of complexes **1** and **3** it has not yet been seen in these experiments. The calculated zero field splitting (ZFS) of the lowest triplet T_1(A) is also given.

We are therefore motivated to understand the changes in PLQY caused by substitutions on the ligand in complexes **1**−**4**. In particular it is important to note that there are two competing contributions to the PLQY: radiative decay and nonradiative decay. In this paper we will focus on understanding the differences in the radiative decay of these four iridium(III) complexes. We will show that these can be understood in terms of the interplay between SOC and the changes in electronic structure caused by chemical substitutions.

There have been few reported attempts to understand the role of SOC in phosphorescent iridium(III) complexes in particular for blue emissive materials. Previous work has focused on the green phosphorescent complex *fac*-tris(2-phenylpyridyl)iridium(III), [Ir(ppy)$_3$]. Hofbeck and Yersin[14] identified three close lying excited states from low temperature spectroscopic measurements as the zero field split sublevels of the lowest triplet excitation, T_1. Ir(ppy)$_3$ has C_3 symmetry, and one expects SOC to split a nonorbitally degenerate triplet state into a nondegenerate (A) state and a 2-fold degenerate (E) state, with the A state having slightly lower energy.[15] It is therefore interesting that Hofbeck and Yersin found three distinct states, none of which were split by a magnetic field, suggesting that they are all nondegenerate. Thus, Hofbeck and Yersin argued that the C_3 symmetry is lifted by solvent effects. Interestingly, a number of in vacuo density functional calculations[16,17] suggest that the symmetry of the iridium(III) complex is lower in the T_1 state than in the ground state, S_0. Since the symmetry lowering can occur in equivalent ways because of the 3-fold symmetry of the S_0 state, this results in the existence of equivalent minima on the T_1 potential energy surface.

The three level substructure observed in the emitting "triplet" manifold of Ir(ppy)$_3$ has similarities to the related d^6 systems Ru(bpy)$_3^{2+}$ and Os(bpy)$_3^{2+}$.[18−20] The existence of three nondegenerate states implies lower symmetry than the ground state (D_3) in these cases. With isotopic substitution in suitable host lattices it is possible to investigate whether the excited emitting states correspond to a localization of the metal-to-ligand charge transfer (MLCT) state onto one ligand using high resolution spectroscopy.[21] The driving force for this low symmetry distortion (vibronic coupling) and the interaction with the environment is beyond the scope of this work. A major difference between the Ru and Os systems and the Ir complexes of the present study is the greater influence of the SOC in mixing singlet character into the lowest T_1 state, because of both the larger SOC constant for Ir and the changes in the energies of the singlet−triplet levels (discussed below).

A number of groups have studied relativistic effects theoretically.[16,17,22−28] Most approaches taken have included SOC perturbatively. We have recently shown[28] that this approximation accurately reproduces the results of calculations in the two-component formalism, which includes SOC to all orders, in these complexes. We have also shown that scalar relativistic effects are sizable in these iridium(III) complexes, and play a key role in determining the degree of MLCT character and hence their optical properties.[27] Both Matsushita et al.[23] and Jansson et al.[17] studied Ir(ppy)$_3$ with SOC included via the semiempirical effective nuclear charge method, which includes SOC on top of nonrelativistic calculations. Matsushita et al.[23] studied the mixing of singlet and triplet states and the implications of this for phosphorescence, and Jansson et al.[17] investigated the nature of the T_1 excitation in some depth. Nozaki et al.[16,29] have also investigated organometallic complexes with the SOC included perturbatively about nonrelativistic TDDFT calculations. It was shown[16] that this method provides a reasonable description of the zero-field splittings and oscillator strengths of Ir(ppy)$_3$, and in a further study Nozaki and collaborators investigated the differences in the optical properties in a range of tris(2,2′-bipyridine) transition metal complexes using the same method.[29]

Trends across related molecules can also provide important insights into the role of SOC in iridium(III) complexes. Li et al.[30] pointed out that, to leading order in perturbation theory, the radiative rate from T_1 is proportional to the inverse square of the energy gap between T_1 and S_1. Haneder et al.[31] also discussed this effect but found poor agreement with experiment. However, Jacko et al.[32−34] have recently found that an additional dependence on the energy gap between T_1 and S_1, which is also inverse square to leading order, arises from the details of the hybridization between ligand-centered (LC) and MLCT excitations required to form T_1. Thus Jacko et al.'s[33] work predicts that the radiative rate of T_1 varies as the fourth power of the inverse of the energy gap between T_1 and S_1.

EXPERIMENTAL SECTION

Synthesis and Characterization. The synthesis and characterization of complexes **1**, **2**, and **4** has been previously reported by Lo et al.[10] **3** was prepared by a similar synthetic method, details of which are given in the Supporting Information. Oxidation potentials were determined by cyclic voltammetry in dichloromethane and referenced against the ferricenium/ferrocene couple (Supporting Information).[10]

Experimental Method. Magnetic circular dichroism (MCD) experiments were performed at 10 K and an applied 5 T magnetic field. The iridium(III) complexes were dissolved in 2-methyltetrahydrofuran, which was chosen for its capacity to form high quality glasses suitable for low temperature MCD measurements. The total and differential circularly polarized light intensities were measured simultaneously using a single beam instrument consisting of a xenon arc lamp dispersed by a Jobin/Yvon 750 S monochromator. The beam

dx.doi.org/10.1021/ic201899z | Inorg. Chem. 2012, 51, 2821−2831

was linearly polarized by a calcite crystal (extinction $<10^{-6}$), mechanically chopped at 500 Hz (New Focus 3501), circularly polarized by a photoelastic modulator at a frequency of 42 kHz (Hinds PEM II/IS42), and passed through the sample held in an Oxford Instruments Spectromag 7 T superconducting magnet. Light was detected with either an S-5 photomultiplier (Hamamatsu R7459) or a Si avalanche photodiode detector. All instrument control and data collection was achieved with GPIB protocols and LABVIEW software. Emission spectra were collected using the 350.7 nm line of a Kr^+ laser and a SPEX1704 monochromator.

MCD is the differential absorption of left and right circularly polarized light in the presence of a magnetic field.[35] MCD spectra can be analyzed in terms of the so-called A, B, and C-terms. A and C-terms arise from degeneracy in the excited or ground states respectively, while B-terms are from mixing between electronic states or changes in the total angular momentum. MCD A-terms appear as a derivative line shape in the spectra, owing to spectral overlap between degeneracies lifted by the magnetic field (see Supporting Information, Figure S1). C-terms appear as a single band, but because of their ground state degeneracy, C-terms are temperature sensitive. B-terms also appear as single bands, but show no temperature dependence as the line shape is not determined by degenerate states.

Computational Method. The measured[10] crystal structure of **1** was used as the initial input for the geometry optimization. The *n*-propyl groups were removed from the ligands since they have only a weak inductive effect and are unlikely to affect the electronic structure significantly and will complicate the potential energy surface. The structures of **1**−**4** were relaxed via density functional theory (DFT) using the B3LYP hybrid functional[36−38] in the GAMESS suite of programs.[39,40] These calculations used a LANL2DZ basis[41] for the iridium and 6-31G basis for hydrogen, carbon, nitrogen, and fluorine.[42,43] Motivated by our MCD results, see Results and Discussion, care was taken to conserve the C_3 symmetry of these *facial* complexes throughout the geometry optimization procedure. The converged molecular structures changed little from measured crystal geometries (see Supporting Information).

Time-dependent DFT (TDDFT) property calculations were carried out with the Amsterdam Density Functional (ADF2009.01) program.[44−46] As with the geometry optimization, the B3LYP hybrid functional was used. On the basis of the one-component zeroth order regular approximation (ZORA),[47,48] the 50 lowest scalar relativistic singlet and triplet excitations were calculated. SOC was included perturbatively around the one-component TDDFT calculations,[49] leading to a total of 200 spin-mixed excitations. The calculations were performed with a Slater type TZP basis set[50,51] and a frozen core approximating the iridium [1s 2s 2p 3s 3p 3d 4s 4p 4d 4f], fluorine [1s], nitrogen [1s] and carbon [1s] shells. Nonrelativistic calculations were also carried out for comparison.

Extensive benchmarking calculations have shown that the choice of basis set has a large effect on the calculated energies and that the TZP basis is the minimum required to get good agreement with experiment.[28] Treating the core electrons on the iridium atom within the frozen core approximation has little effect on the calculated excitations. Including SOC as a perturbation to the scalar ZORA, TDDFT gives essentially the same results as those obtained from more expensive two-component methods, and is more easily related to the underlying molecular orbital excitations.[28]

C_3 molecular symmetry could not be utilized in the ADF TDDFT calculations because the C_3 point group contains complex irreducible representations. As a result small splittings between formally degenerate excitations can occur (cf. Supporting Information) despite the C_3 symmetry of the input geometry. These small splittings are artifacts of the calculation and have no physical significance. Symmetry labels were determined manually by examining the full range of properties of the excitations.

To investigate the total redistribution of charge after successive fluorination, the molecule was divided into three fragments comprising the iridium, phenyl, and triazolyl moieties. A Hirshfeld population analysis was performed according to these divisions.[52]

SOC mixes singlet and triplet states. It is well-known that TDDFT favors low-spin states over high-spin states because of the approximate treatment of the exchange interaction.[53−55] Thus, triplet excitations will tend to be destabilized relative to singlets. This may have two important consequences for our results: in the scalar relativistic DFT this will shift the energies of the excitations as described above; further this will lead to an overestimation of the degree of hybridization between singlets and triplets because of SOC. Quantifying these errors is beyond the scope of this work; however, a rough estimate might be made by comparing to Dirac−Hartree−Fock calculations as the Hartree−Fock approximation displays the opposite bias.[53]

RESULTS AND DISCUSSION

Degeneracy and Symmetry. The absorption and MCD of complexes **1**−**4** share many similarities (Figure 2). Only low temperature measurements will be discussed below; however, many of the features are still present at room temperature but are, as might be expected, considerably broadened and therefore poorly resolved.

In the MCD spectra between 2.7−3.2 eV a number of features can be clearly identified. The MCD spectra continue above 3.2 eV but because of the strong optical absorption the spectra become noisy and unreliable. It is clear that the higher energy absorptions beyond 3.2 eV are the result of a complex ensemble of excitations, so it is not clear that MCD data in this region provides significant insight into the electronic structure. Further, these higher lying states (>0.5 eV above the absorption onset) are of little significance to the emission mechanism at room temperature.

The first feature to note in the MCD is the strong A-term localized just after the absorption onset. The peak energy of the corresponding absorption band is reported in Table 2. In all the complexes the A-term feature has similar intensity.

It is interesting to compare this result with Hofbeck and Yersin's spectroscopic studies of $Ir(ppy)_3$, which shares many similarities with complexes **1**−**4**.[28] On the basis of these measurements Hofbeck and Yersin argued that in $Ir(ppy)_3$ the lowest triplet excitation, T_1, is split into three substates. This led them to postulate that the symmetry of $Ir(ppy)_3$ is lowered from C_3 by distortions induced from a host material, whether a solvent or a solid matrix.[14,56] Indeed this group has argued that spectroscopic measurements reveal three distinct substates of T_1 in many iridium(III) complexes.[56−59]

Therefore, the clear resolution of MCD A-terms in all four complexes is an interesting result. While an A-term is due to an excited state degeneracy, the degree of degeneracy is only established within the line width of the feature. These linewidths are comparable with the observed splitting in $Ir(ppy)_3$,[14] but the clear equal and opposite signed peaks observed in Figure 2 indicates that the "pseudo A-term" must arise from the 2E state at C_3 symmetry. That is, any symmetry lowering does not split the E levels of the lowest T_1 manifold enough to destroy the derivative shaped $\Delta\varepsilon$ expected for an A-term from a degenerate E state. The symmetric shape of this MCD feature is maintained at all field strengths and so is not a result of (B-term) magnetic field mixing. Therefore, the observed MCD A-term must be due to excitation into the (degenerate) E electronic substate of the first triplet state in C_3 (or to excitation into two close lying levels that originate from an E state, but that cannot be resolved in these experiments.) Further, a clear mirror image symmetry is observed between the lowest energy observed feature in absorption and the highest energy observed feature in emission (Figure 3). The relatively small Stokes shift ($\sim$220 cm^{-1}) is consistent with the observed lowest energy absorption feature also being responsible for the emission. At temperatures $\gtrsim$10 K most of the emission is coming from the E manifold, the same state which

dx.doi.org/10.1021/ic201899z | Inorg. Chem. 2012, 51, 2821−2831

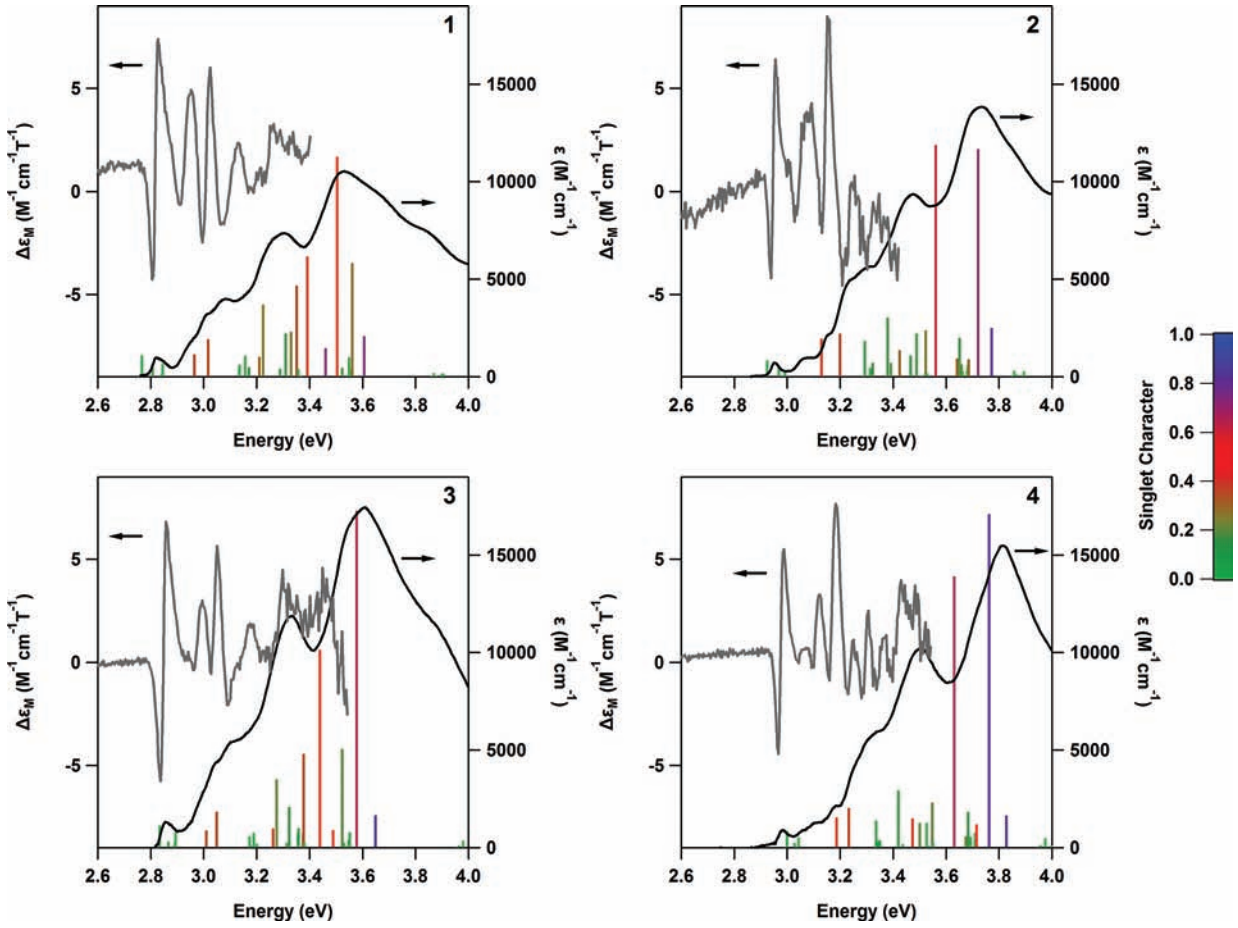

Figure 2. Low temperature absorption, MCD, and calculated relativistic TDDFT excitations (which include SOC perturbatively) for iridium(III) complexes **1**−**4**. ε is the usual molar extinction coefficient while $\Delta\varepsilon_M$ is the MCD extinction coefficient scaled to the magnetic field strength. The calculated excitations are color-coded according to the degree of singlet character. In all the complexes, a strong MCD A-term occurs around the first absorption band.

Table 2. Measured Optical Energy Gaps from Low Temperature Absorption Spectroscopy, Oxidation Potentials from Cyclic Voltammetry,[10] and the Orbital Energies from Scalar Relativistic DFT Calculations[a]

	experimental		calculated energy (eV)						
complex	E_{opt} (eV)	$E_{1/2}$ (ox) (V)	HOMO-1	HOMO	LUMO	LUMO+1	$\Delta E_{HOMO-HOMO-1}$	$\Delta E_{LUMO-HOMO}$	$\Delta E_{LUMO+1-LUMO}$
1	2.82	0.28	−5.154	−4.980	−1.166	−0.989	0.174	3.814	0.177
2	2.95	0.50	−5.583	−5.393	−1.405	−1.229	0.190	3.988	0.176
3	2.85	0.50	−5.544	−5.382	−1.489	−1.335	0.162	3.893	0.154
4	2.98	0.72	−5.969	−5.781	−1.701	−1.557	0.188	4.080	0.144
(**1** + **4**) − (**2** + **3**)	0.00	0.00	0.004	0.014	0.027	0.018	0.010	0.013	−0.009

[a]The row labelled (**1**+**4**)−(**2**+**3**) is a test of eq 6, formally, $(\Pi_1 + \Pi_4) - (\Pi_2 + \Pi_3)$. Hence, an entry of 0 indicates perfect agreement between experiment/DFT and the predictions of that equation. The observation that entries of this row are all zero to a very high accuracy indicates that the changes to the excitation energies caused by fluorination at the X and Y positions act independently of one another.

carries the absorption intensity. At low temperature (2 K) the emission changes dramatically as the upper levels are depopulated. Similar to that described for $Ir(ppy)_3$,[14] a Herzberg−Teller vibronically allowed emission is observed and this, together with the magnetic circular photoluminescence, will be the subject of a future publication.[60]

At energies above the first A-term two positive bands can be identified in the MCD spectra (cf. Figure 2). It is not possible to definitively label these features as arising from particular MCD terms using the experimental data alone, although it is clear that a number of B and A-terms are clearly required to describe the spectrum.

Relativistic Electronic Structure Calculations: Comparison with Spectroscopy. To further understand the MCD spectra we carried out relativistic TDDFT calculations. These calculations give us information at three levels of theory: (i) scalar relativistic DFT, these are the simplest calculations to understand and interpret as they fit most closely with chemical intuition about molecular orbitals; (ii) scalar relativistic TDDFT, these calculations give us access to what the excited states of the complexes would be in the absence of SOC and can allow us to understand the excitations in terms of transitions between the orbitals in the scalar relativistic DFT calculations; and (iii) perturbation theory with SOC about the scalar relativistic TDDFT.

dx.doi.org/10.1021/ic201899z | Inorg. Chem. 2012, 51, 2821−2831

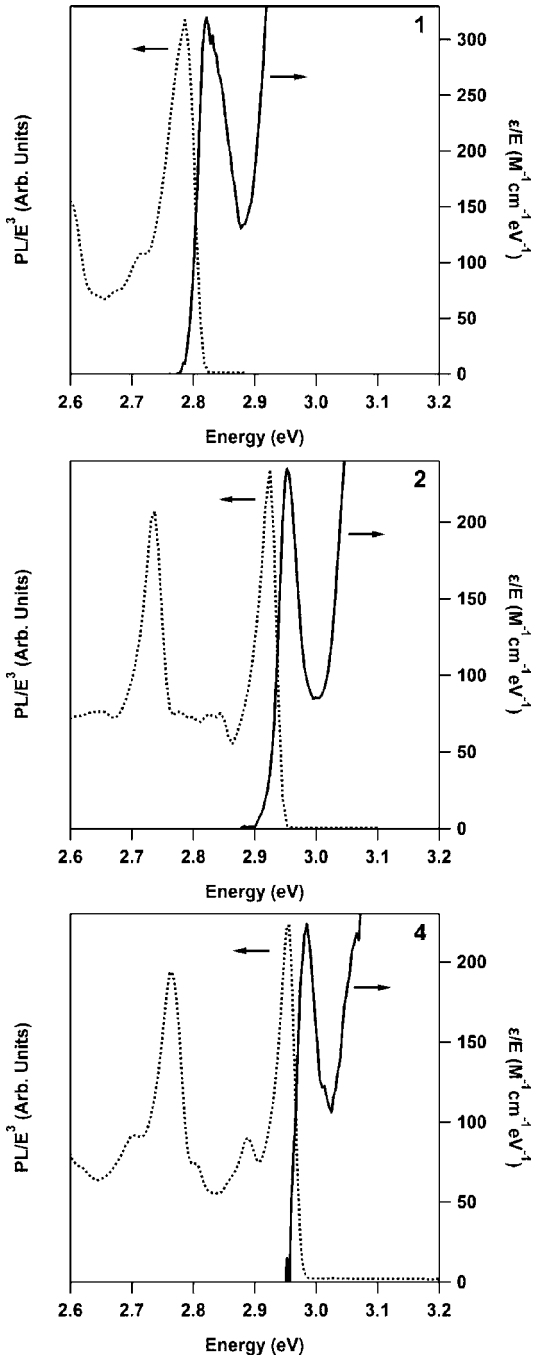

Figure 3. Plots of the absorption and emission of complexes **1**, **2**, and **4** at 10 K. The absorption and emission axes have been rescaled according to the energy and energy cubed, respectively. Similar spectra are obtained at temperatures above 10 K, but are significantly broader and poorly resolved.[10,27] All three complexes show clear mirror image symmetry, indicating that the state responsible for the observed lowest energy absorption is also responsible for the emission at this temperature.

The latter calculations are the most accurate and are directly comparable to experiment, and also allow an understanding of these transitions in terms of the scalar relativistic TDDFT. Full results of all three levels of theory are tabulated in the Supporting Information.

We will focus initially on the calculations that include SOC and a comparison of these with experiment. We have previously shown that this level of theory gives good agreement with full two-component ZORA calculations for iridium(III) complexes, despite its much lower computational cost[28] and therefore we expect good agreement with experiment.

The vertical lines in Figure 2 show the calculated excitation spectrum: the heights of the lines indicate the calculated oscillator strengths and the colors indicate the degree of singlet character of the excitations (because of the mixing of singlets and triplets by SOC). The calculations accurately reproduce the experimentally measured absorption spectrum. In the Supporting Information, Figure S2 we compare calculated spectra that have been convoluted with bandshapes of finite width, making the agreement with experiment even more clear. In particular, the absorption onset and peak energies are very closely reproduced. Further, the relativistic TDDFT calculations provide an accurate prediction of the energy at which light is emitted.

SOC splits the first triplet state $T_1(A)$ (we include the label A to stress that there is no orbital degeneracy as the orbital part of this state transforms according to the A irreducible representation of C_3) into a nondegenerate A and 2-fold degenerate E spin−orbit states (which we will henceforth refer to as 1A and 2E). The calculated zero field splitting (ZFS) of $T_1(A)$ is presented in Table 1. The lowest energy state, 1A, is predicted to have a very small oscillator strength ($<10^{-5}$ au) in all four complexes. Four higher energy excitations (two A and two E; numbered 3−6) lie above the $T_1(A)$ manifold because of the ZFS of the second triplet state $T_2(E)$ (Figure 4).

In light of the calculated excitations we may begin to assign the MCD spectrum. The lowest energy MCD A-term feature can be assigned as originating from the transitions to the 2E levels. If there is a symmetry lowering perturbation as occurs in $Ir(ppy)_3$ and similar systems as discussed above the levels are split by less than the line width of the spectral features. The calculated oscillator strength of the transition to the 2E state is similar across all four complexes as is the observed MCD signal. It is also the strongest excitation in the entire manifold of $T_1(A)$ and $T_2(E)$ excitations (Figure 4). The negligible oscillator strength predicted for 1A in all complexes is consistent with this first A-term being the lowest energy observable feature in the MCD and with the energy of this feature coinciding with the absorption onset.

Higher energy excitations 7A and 8E coincide with the strong MCD features between 2.9 and 3.2 eV, which allows their assignment to an MCD B-term followed by an A-term (Figure 2). This pair of excitations arises from a complex mix of scalar excitations with no one singlet or triplet excitation dominating. Above ∼3.2 eV the density of states becomes much greater and unambiguous identification of MCD features is difficult. However, as noted above, these states are not important for the emissive properties of the complexes at room temperature.

Temperature Dependence of Radiative Rates. Note that the above assignments predict that 1A does not play a significant role in the absorption of light by these complexes. It is clearly interesting, given the potential optoelectronic applications of these complexes, to ask what role excitation 2E, and more generally all of the excited states, play in the emission of light. To examine this question we will assume that the vibration relaxation from the initially excited state achieves thermal equilibrium. The fractional Boltzmann probability, $p_i(T)$, of an

dx.doi.org/10.1021/ic201899z | Inorg. Chem. 2012, 51, 2821−2831

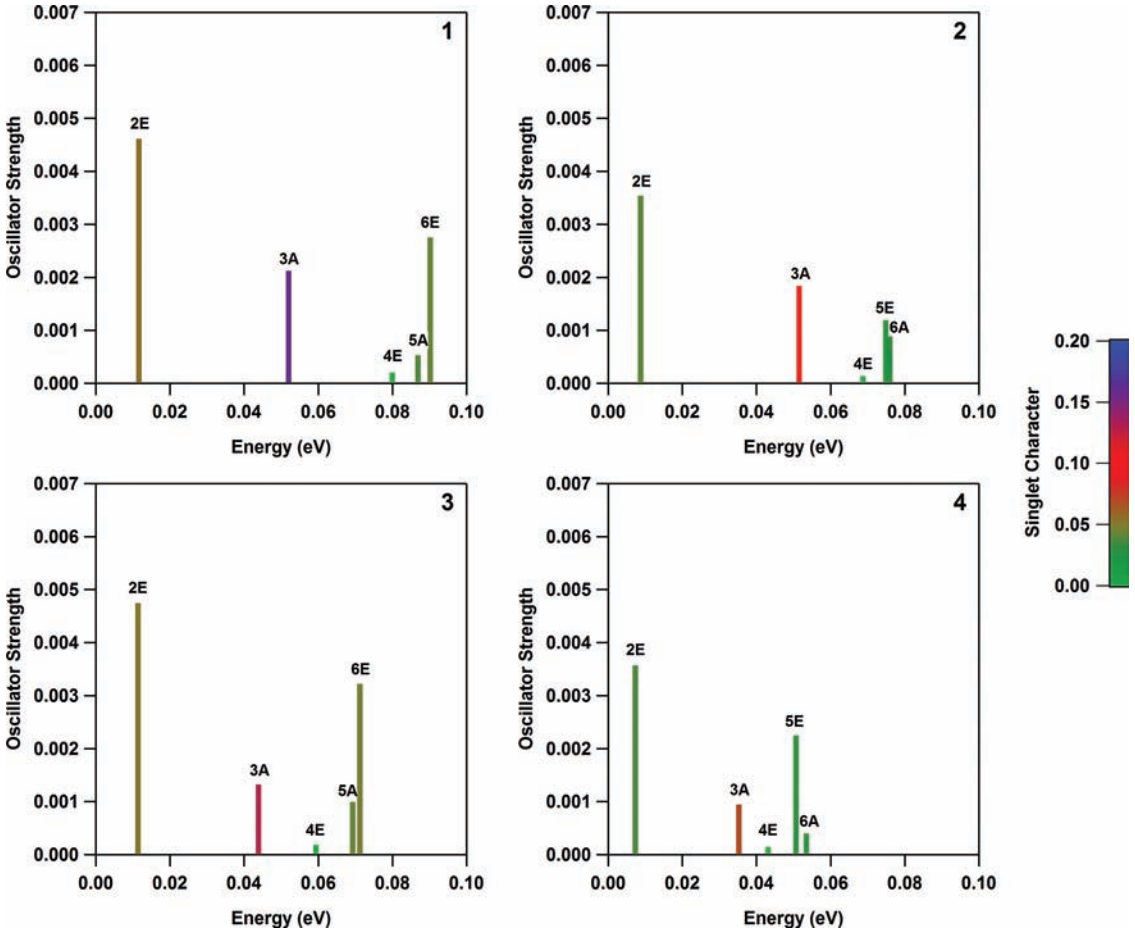

Figure 4. Lowest six excitations of iridium(III) complexes **1**−**4** calculated from SOC perturbation TDDFT with the complexes constrained to C_3 symmetry. Plotted with respect to the energy of the first excitation 1A [which has an extremely small ($f < 10^{-5}$ au) oscillator strength], the energy range between excitations 1 and 6 decreases with fluorine substitution. The ZFS of the T_2 manifold (excitations 3−6) is also reduced by fluorination. Note that the color coding indicating the singlet character has been rescaled, compared to Figure 2, to emphasize the small differences in singlet character.

excited complex being in the *i*th excited state at temperature T is given by

$$p_i(T) = \frac{g_i e^{-(E_i - E_{1A})/k_B T}}{\sum_j g_j e^{-(E_j - E_{1A})/k_B T}} \quad (1)$$

where g_i is the degeneracy, E_i is the energy, k_B is Boltzmann's constant, and E_{1A} is the energy of the lowest energy excitation, 1A. Thence, the probability $P_i(T)$ that a detected photon was emitted from excitation i is given by

$$P_i(T) = \frac{p_i(T)k_i^R}{\sum_j p_j(T)k_j^R\left(\frac{k_i^R + k_i^{NR}}{k_j^R + k_j^{NR}}\right)} \approx \frac{p_i(T)k_i^R}{\sum_j p_j(T)k_j^R} \quad (2)$$

where k_j^R and k_j^{NR} are, respectively, the radiative and nonradiative rates from the *j*th level, and the final approximation holds if there is sufficiently little variation in the total decay rates across all states with a significant thermal population, $p_i(T)$, at a given temperature, which we expect not to induce large errors because the measured total radiative rates are the same magnitude as the measured radiative rate.[10] Radiative rates and lifetimes were calculated from the TDDFT results via the Stickler−Berg relation.[61,62] The predictions of eq 2 for

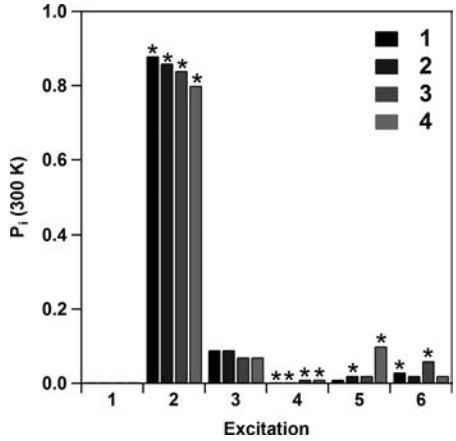

Figure 5. Zeroth order probability, P_i(300 K), of observing emission from iridium(III) complexes **1**−**4** for the lowest six excitations calculated from SOC perturbation TDDFT. At room temperature the probability of observing emission from 1A is close to zero. Degenerate, E, excitations are denoted by an *.

all four complexes at 300 K are reported in Figure 5. In particular we find that to leading order, at 300 K, ≥80% of the emission comes from 2E in all four complexes. The vanishingly small probability of emission from 1A suggests that the bulk of the

dx.doi.org/10.1021/ic201899z | Inorg. Chem. 2012, 51, 2821−2831

emission does not occur from the lowest excited state level in these complexes at temperatures ≥10 K; this result is highly robust to higher order corrections in $(k_i^R + k_i^{NR})/(k_j^R + k_j^{NR})$.

The calculations also predict that the lowest state with significant absorption (2E) is also responsible for the bulk of the emission at temperatures where this state has a significant thermal population (specifically above about 10 K). This is responsible for the mirror image symmetry between absorption and emission spectra as neither the absorption nor the emission processes involve the lowest energy excited state. Therefore, theory predicts that these complexes will display mirror image symmetry at $T \geq 10$ K. The mirror image rule is indeed obeyed experimentally as shown by the results shown in Figure 3. This is strong experimental evidence that the excitation responsible for the MCD A-term and the absorption onset (2E) also dominates the emission process at temperatures greater than ∼10 K.

The calculated radiative lifetime of all four complexes reveals very similar temperature dependent profiles (Figure 6), which

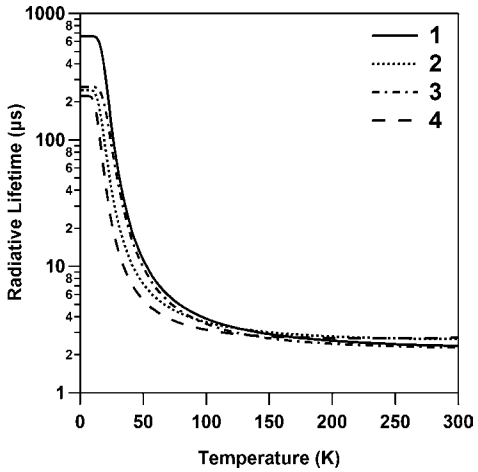

Figure 6. Temperature dependence of the radiative lifetimes of iridium(III) complexes **1**−**4** predicted from SOC perturbation TDDFT excitations. Below 10 K only the lowest state 1A has significant population and so the radiative lifetime is long and plateaus. At 300 K complexes **1** and **3**, which have protons at the Y position, have similar lifetimes, as do complexes **2** and **4**, which have fluorines at the Y position.

closely resembles the measured total lifetime of many similar iridium(III) complexes.[14,58,63] Below ∼10 K the radiative lifetime plateaus, as the lowest energy state, 1A, is essentially fully populated. As the lowest state has such weak oscillator strength even a slight change in the calculated oscillator strength for this state will have a dramatic effect on the final lifetime at low temperature.[28] The true radiative rate at low temperature is likely to be enhanced by Herzberg−Teller (HT) coupling, which is not included in our calculations but may well give rise to a radiative rate larger than, or of a similar magnitude to, the calculated direct radiative rate. Nevertheless we expect the qualitative shape of the curves in Figure 6 to be correct although the intercepts may be somewhat lower.

Although most of the light is emitted from 2E, a substate of T_1(A), the occupation of the T_2(E) states may still have important consequences for the optoelectronic properties of these complexes. Figure 4 shows that fluorination leads to important changes in properties of the T_2(E) manifold:

First, relative to the energy of the first excitation, 1A, the T_2(E) manifold of excitations (3−6) shifts down in energy following fluorine substitution (Figure 4). This can be understood by considering the scalar relativistic TDDFT calculations where the energy separation between the T_1(A) and T_2(E) excitations is also reduced with fluorine substitution (see Supporting Information). These low energy excitations are formed almost exclusively from transitions between the frontier orbitals. In all complexes T_1(A) is primarily composed of HOMO→LUMO (>62%) and HOMO-1→LUMO+1 (>15%) transitions, whereas T_2(E) is made up of HOMO→LUMO+1 (>47%) and HOMO-1→LUMO (>11%) transitions (see Supporting Information). The changes in excitation energy can be traced back to the effects that fluorination has on these orbital energies. Specifically, if we examine the orbital transitions with the greatest contribution in the T_1(A) and T_2(E) excitations (HOMO→LUMO and HOMO→LUMO+1, respectively), the energy separation between the T_1(A) and T_2(E) excitations is dependent on the LUMO−LUMO+1 energy gap. In order of complexes **1**−**4** the LUMO−LUMO+1 energy separation decreases (Table 2) consistent with the calculated decrease in the T_1(A)−T_2(E) separation (Table 1).

Second, the predicted overall splitting of the T_2(E) excitation manifold (excitations 3−6) decreases with fluorination, from a maximum of 38 meV for **1** to 18 meV for **4** (Figure 4).

These two effects have important consequences for the occupation of the T_2 manifold. In the parent complex, **1**, an excitation only has a Boltzmann probability of 12% of being in the T_2 manifold at room temperature (Supporting Information, Figure S3). This probability rises to 15% in **2**, 20% in **3**, and 29% in **4**. Excitations 3−6 all have weaker oscillator strengths (and therefore slow radiative rates) compared to 2E, so this is our first clue to why fluorination lowers the radiative rate of the complexes at room temperature.

Moreover, this redistribution of spectral weight may also be important for the nonradiative rate. The increase in the population of the T_2 manifold is much larger for fluorination at the X position (which takes **1**→**3** and **2**→**4** and increases the occupation of the T_2 states by a factor of 2) than for fluorination at the Y position (which takes **1**→**2** and **3**→**4**). Although we have not calculated or measured the nonradiative decay rates for individual excitations, it is reasonable to expect that, because they are embedded in the vibrational bands based on the lower T_1 state, the T_2 states may have much higher nonradiative decay rates than the T_1 states. This would then give a natural explanation of why fluorination at the X position increases the nonradiative decay rate much more dramatically than fluorination at the Y position does.

It is interesting to note that the redistribution of spectral weight is not simply an effect of the blue shift. **2** is shifted further to the blue than **3** (Figure 2) yet the population of the T_2 manifold is only 15% in **2**, compared to 20% in **3**.

Linear Response to Fluorination. We will now demonstrate that fluorination at the X and Y positions act independently. To do this we compare a wide range of measured and calculated properties of complexes **1**−**4**. Let us assume initially that fluorination causes a *small* shift in some property, Π, of the complex. The assumption of the small shift allows us to develop a linear response theory[64] for chemical substitution. If we denote the change in Π caused by fluorination at the X position by $\delta\Pi_X$ and the change in Π caused by fluorination at

dx.doi.org/10.1021/ic201899z | Inorg. Chem. 2012, 51, 2821−2831

the Y position by $\delta\Pi_Y$, then the assumption of linearity leads directly to the prediction that

$$\Pi_2 = \Pi_1 + \delta\Pi_Y \quad (3)$$

$$\Pi_3 = \Pi_1 + \delta\Pi_X \quad (4)$$

$$\Pi_4 = \Pi_1 + \delta\Pi_X + \delta\Pi_Y \quad (5)$$

where Π_n is the value of the property Π for the nth complex. Note that **1** is unfluorinated, **2** is fluorinated only at the Y position, **3** is fluorinated only at the X position, and **4** is fluorinated at both the X and Y positions. Thus, we have

$$\Pi_1 + \Pi_4 = \Pi_2 + \Pi_3 \quad (6)$$

Where the property Π is clear from context, it will be useful to introduce the shorthand $(1 + 4) - (2 + 3) = 0$ to summarize eq 6.

The eq 6 is potentially quite general for different families of molecules and where substitutions cause sufficiently subtle effects in some measured property. We will show below that a range of important properties in complexes **1**−**4** display this behavior. Therefore, it may be possible to use this as a design principle for tailoring the properties of organometallic complexes to specific applications.

In Table 2 we report the experimentally measured optical excitation and oxidation potentials (reversible reduction potentials could not be determined for comparison) of complexes **1**−**4**. The gap between the highest occupied molecular orbital (HOMO) and the lowest unoccupied molecular orbital (LUMO) calculated from scalar relativistic DFT calculations (upon which the TDDFT and SOC perturbation calculations are based) follows the trend observed spectroscopically, although, unsurprisingly, it vastly overestimates the measured optical gap (Table 2). Nevertheless, for all three of these properties, we find that eq 6 holds to a very high accuracy.

Analysis of the fragment charge distribution (Table 3) shows the effect of fluorination more clearly. The successive addition of fluorine promotes the redistribution of charge from the triazolyl ring toward the phenyl ring. Here one sees that the relationship $(1 + 4) - (2 + 3) = 0$ with fluorination very clearly. This indicates that redistributions of charge caused by fluorination at the X and Y positions are uncorrelated.

Table 3. Partial Charge Per Fragment Based on Hirshfeld Population Analysis from Scalar Relativistic DFT[a]

fragment	1	2	3	4	$(1 + 4) - (2 + 3)$
iridium	0.4383	0.4417	0.4086	0.4130	0.0010
triazolyl	0.0368	0.0360	0.1391	0.1392	0.0009
phenyl	−0.4705	−0.4731	−0.5461	−0.5482	0.0005

[a]The total charge distribution changes with fluorination as electron density is redistributed from the triazolyl to the phenyl ring. The column labelled $(1 + 4) - (2 + 3)$ is a test of the sum rule for fluorination, eq 6, where an entry of 0 indicates perfect agreement between the Hirshfeld population analysis and the predictions of that equation. The observation that entries of this row are all zero to a very high accuracy indicates that redistributions of charge caused by fluorination at the X and Y positions are independent of one another.

One can also observe the $(1 + 4) - (2 + 3) = 0$ rule in relativistic effects. In all complexes, states arising from the $T_2(E)$ manifold remain predominantly triplet in character (>95%), apart from the 3A state, which has a significant component of singlet character because of the $S_1(A)$ manifold. In complex **1** the singlet character of 3A reaches 16%, but fluorination reduces the singlet component to 10% and 13% for **2** and **3**, respectively (see Supporting Information). The difluorinated complex **4** has the lowest singlet component in 3A with only a 7% contribution. Again the same linear response to fluorination is observed.

At 300 K the radiative rates of complexes **1**−**4** are calculated to be 4.3×10^5, 3.8×10^5, 4.4×10^5, and 3.7×10^5 s^{-1}, respectively, which is the same order of magnitude as measured experimentally (Table 1).[10] Complexes **1** and **3** have similar radiative rates as do complexes **2** and **4**. This suggests that the important difference, in terms of radiative rates, is whether the Y position is protonated (as in complexes **1** and **3**) or fluorinated (as in complexes **2** and **4**). The same trend is observed in the experimentally measure radiative rates (Table 1). Conversely, the experimental data shows that fluorination at the X position increases the nonradiative rate by more than an order of magnitude, whereas fluorination at the Y position has a much smaller effect on the k_{nr}.

Mechanism of Changes in the Radiative Rate Due to Fluorination. Phosphorescence occurs because SOC mixes singlets and triplets. This mixing is reduced as the energy gap between the relevant singlets and triplets is increased. In a related series of complexes one expects the radiative rate to depend on the energy gap between a triplet and the singlet with which it mixes.[30,32,58,42] Li et al.[30] pointed out that the rate depends on the inverse square of this gap at the lowest order in perturbation theory. However, recently Jacko et al.[32−34] have shown that a second inverse square relationship arises because of the hybridization between metal and ligand orbitals. Thus overall the radiative rate should exhibit a quadratic dependence on the inverse of the energy gap between a triplet and the singlet with which it mixes.[33]

As discussed earlier, the complexes studied here predominately emit from the 2E level at room temperature. If we compare the TDDFT results with and without the effects of spin−orbit perturbation (see Supporting Information for full tabulation) we find that in all of the complexes the 2E state is basically a substate of $T_1(A)$ with small but significant contribution from $S_3(E)$ of 5.2%, 4.1%, 5.1%, and 3.7% for complexes **1**−**4**, respectively. It is worth noting that $S_3(E)$ and $S_5(E)$ are the strongest singlet excitations in the MLCT manifold, so it is interesting that a strong excitation like $S_3(E)$ should couple into the lowest triplet more strongly than the closer lying $S_1(A)$ and $S_2(E)$ excitations. This is clearly important for the large radiative rate and hence the high PLQY of, at least, the parent complex (**1**).

The calculated energy gap $S_3(E)$-$T_1(A)$ is strongly dependent on fluorination at the Y position: this gap is ∼10% larger in complexes **2** and **4** (where Y = F) than in complexes **1** and **3** (where Y = H). However, fluorination at the X position has little effect on the $S_3(E)$-$T_1(A)$ gap. In Figure 7 we compare the calculated $S_3(E)$-$T_1(A)$ gap with the calculated radiative rates. The data is consistent with the prediction of Jacko and Powell[33] that the radiative rate decreases as the fourth power of the $S_3(E)$-$T_1(A)$ energy gap (Figure 7).

Therefore, the question becomes why does fluorination increase the $S_3(E)$-$T_1(A)$ gap? To understand this, it is helpful to compare the scalar relativistic DFT and TDDFT calculations. In the Supporting Information we tabulate the largest contributions to each TDDFT excitation in terms of transitions between DFT molecular orbitals. We find that, in all four complexes, $T_1(A)$ is predominately a HOMO→LUMO

dx.doi.org/10.1021/ic201899z | Inorg. Chem. 2012, 51, 2821−2831

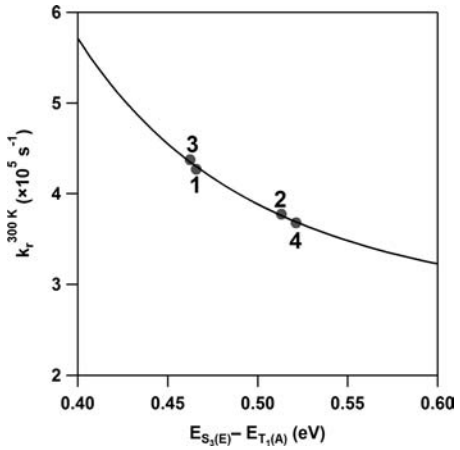

Figure 7. Calculated total radiative rate at 300 K for iridium(III) complexes **1**−**4**, plotted against the calculated energy gap between the scalar TDDFT excitations $S_3(E)$ and $T_1(A)$. The $S_3(E)$-$T_1(A)$ energy gap is found to be strongly dependent on the fluorination at the Y position, whereas fluorination at X does not change the relative energy separation significantly. The line is a best fit for the predicted dependence between the inverse fourth power of the radiative rate and the singlet−triplet energy gap.[33] The calculated radiative rate is the same order of magnitude as the experimentally measured rate.[10]

transition (with weights of 72%, 66%, 69%, and 62% in complexes **1**−**4**, respectively) and $S_3(E)$ is dominated by the HOMO-1→LUMO transition (with weights of 94%, 96%, 94%, and 97% in complexes **1**−**4**, respectively). Note that both of these weights obey the $(\mathbf{1} + \mathbf{4}) - (\mathbf{2} + \mathbf{3}) = 0$ rule and that in both cases fluorination at the Y position has a greater effect than that at the X position.

On the basis of the above analysis one expects that, to leading order, the main effect of fluorination on the $S_3(E)$-$T_1(A)$ energy gap, and hence on the radiative rate, is therefore to increase the energy gap between the HOMO and HOMO-1. (One might also ask if there is an effect on the strength of the exchange interaction, but we will not consider this here.) In Table 2 we have listed the energies of the frontier orbitals. The energy gap between the HOMO and HOMO-1 clearly obeys the $(\mathbf{1} + \mathbf{4}) - (\mathbf{2} + \mathbf{3}) = 0$ rule. Although these complexes have C_3 symmetry, the iridium(III) atom sits in an approximately octahedral environment formed by the covalent bonds to the carbon atoms and the dative bonds to the nitrogen atoms. If this octahedral symmetry were exact the HOMO (A) and HOMO-1 (E) would form a triply degenerate T_{2g} manifold. This is responsible for the marked similarities between the HOMOs and (HOMO-1)s of homoleptic iridium(III) complexes.[27,28]

Fluorination at the Y position (**1**→**2**, **3**→**4**) has an important effect on increasing the HOMO−HOMO-1 gap (∼0.2 eV), whereas fluorination at the X position (**1**→**3**, **2**→**4**) has a much smaller effect on the HOMO−HOMO-1 gap. Therefore fluorination at the Y position changes the radiative rate by increasing the degree to which octahedral symmetry is broken, whereas fluorination at the X position only weakly affects this asymmetry. This simple molecular orbital analysis overestimates the magnitude of the increase in the $S_3(E)$-$T_1(A)$ gap because it neglects the other molecular orbital transitions that contribute to $S_3(E)$ and, particularly $T_1(A)$. Nevertheless, this simple molecular orbital picture does correctly reproduce the trend seen in both the relativistic TDDFT calculation with spin orbit coupling and experiment.

Finally, we note that this analysis does not just apply to 2E. For example, the character of 3A is dominated by the combination of the $T_2(E)$ and $S_1(A)$ states. The singlet character of 3A can be directly related to the energy difference between the $T_2(E)$ and $S_1(A)$ states, which in order of the complexes **1**−**4** is 0.20, 0.24, 0.21, and 0.26 eV; these values again satisfy eq 6. As the energy difference between the two states increases, less of the $S_1(A)$ excitation is coupled into 3A.

CONCLUSIONS

The combination of low temperature, high field MCD, absorption and emission spectroscopy with relativistic time-dependent density functional calculations has allowed a rather complete mapping of the low-energy excited states of a family of iridium(III) complexes. This has allowed us to understand the subtle changes induced by fluorination on the experimental spectra and to accurately describe the molecular properties. This has revealed a subtle interplay between the effects of chemical substitutions and SOC and thus photoluminescence efficiency.

The current experiments can be interpreted in terms of C_3 symmetry complexes. No symmetry lowering effects (possible in some excited states because of vibronic coupling and interaction with the environment that would result in localization) are resolved in our measurements. The lowest energy excitation 1A has an extremely small oscillator strength, and as a result transitions to and from the second lowest excitation 2E dominate both the absorption and the emission spectra, respectively, at room temperature (Figure 5). Therefore, a mirror image between absorption and emission is still observed (Figure 3). 2E is a 2-fold degenerate excitation and, as such, is responsible for the distinct MCD A-term found in all complexes (Figure 2).

We have demonstrated that the properties of a family of fluorinated phosphorescent iridium(III) complexes are determined by the independent action of each fluorine substitution (Tables 2 and 3). This independence is demonstrated by the $(\mathbf{1} + \mathbf{4}) - (\mathbf{2} + \mathbf{3}) = 0$ rule, eq 6, which one should expect to hold provided the changes due to a substitution are sufficiently small for a linear response theory to be valid. Therefore, this may represent a general rule to aid the design of new phosphorescent complexes. In this context it is interesting to note (cf. Table 1) that fluorination of the Y position (which takes **1**→**2** and **3**→**4**) reduces the radiative rate by a factor of 2−3; whereas fluorination of the X position (**1**→**3** and **2**→**4**) leads to an order of magnitude increase in the nonradiative rate, but has a much smaller change in the radiative rate.

The calculated radiative lifetime in this family of complexes is found to be dependent on the $S_3(E)$-$T_1(A)$ energy gap, and is consistent with the predicted quadratic dependence on the inverse of the singlet−triplet energy gap. Fluorination at the Y position lowers this gap (Figure 7) and is responsible for suppression of the radiative rate between complexes **1** and **2**, and complexes **3** and **4**. On the other hand, fluorination at the X position does not significantly alter the gap (Figure 7), which explains the similar radiative rates observed in complexes **1** and **3**, and in complexes **2** and **4**. As we have not considered the nonradiative decay mechanisms, we cannot give a full explanation of why fluorinations at the X and Y positions have such different effects on the nonradiative decay rates. However, the fluorination at the X position causes more significant redistribution of the low energy spectral weight: decreasing the T_1-T_2 energy difference by reducing the (LUMO+1)-LUMO gap and decreasing the ZFS of T_2. This reduces the probability

dx.doi.org/10.1021/ic201899z | Inorg. Chem. 2012, 51, 2821−2831

of excitations equilibrating into the main emissive state, 2E, which, it is tempting to speculate, may be related to the dramatic increase in the nonradiative rate.

■ ASSOCIATED CONTENT

Supporting Information

Further details are given in Figures S1−S3 and in tables containing the geometry of optimized structures and transition energies. This material is available free of charge via the Internet at http://pubs.acs.org.

■ AUTHOR INFORMATION

Corresponding Author

*E-mail: p.burn2@uq.edu.au (P.L.B.), bjpowell@gmail.com (B.J.P.).

Notes

The authors declare no competing financial interest.

■ ACKNOWLEDGMENTS

We thank Anthony Jacko and Seth Olsen for helpful conversations. This work was funded by the Australian Research Council (ARC). All calculations were performed on NF-NCI. A.R.G.S. thanks AINSE for a PGRA. P.L.B. and B.J.P. are supported by an ARC Federation Fellowship (FF0668728) and an ARC Queen Elizabeth II Fellowship (DP0877875), respectively.

■ REFERENCES

(1) Xiao, L.; Chen, Z.; Qu, B.; Luo, J.; Kong, S.; Gong, Q.; Kido, J. *Adv. Mater.* **2011**, *23*, 926.
(2) Baldo, M. A.; Lamansky, S.; Burrows, P. E.; Thompson, M. E.; Forrest, S. R. *Appl. Phys. Lett.* **1999**, *75*, 4.
(3) Chou, P. T.; Chi, Y. *Chem.—Eur. J.* **2007**, *13*, 380.
(4) Adachi, C.; Baldo, M. A.; Thompson, M. E.; Forrest, S. R. *J. Appl. Phys.* **2001**, *90*, 5048.
(5) Holder, E.; Langeveld, B.; Schubert, U. *Adv. Mater.* **2005**, *17*, 1109.
(6) Gather, M. C.; Köhnen, A.; Meerholz, K. *Adv. Mater.* **2011**, *23*, 233.
(7) Sasabe, H.; Kido, J. *Chem. Mater.* **2011**, *23*, 621.
(8) Reineke, S.; Lindner, F.; Schwartz, G.; Seidler, N.; Walzer, K.; Lussem, B.; Leo, K. *Nature* **2009**, *459*, 234.
(9) Lo, S.-C.; Harding, R. E.; Shipley, C. P.; Stevenson, S. G.; Burn, P. L.; Samuel, I. D. W. *J. Am. Chem. Soc.* **2009**, *131*, 16681.
(10) Lo, S.-C.; Shipley, C. P.; Bera, R. N.; Harding, R. E.; Cowley, A. R.; Burn, P. L.; Samuel, I. D. W. *Chem. Mater.* **2006**, *18*, 5119.
(11) Lamansky, S.; Djurovich, P.; Murphy, D.; Abdel-Razzaq, F.; Lee, H.-E.; Adachi, C.; Burrows, P. E.; Forrest, S. R.; Thompson, M. E. *J. Am. Chem. Soc.* **2001**, *123*, 4304.
(12) You, Y.; Park, S. Y. *Dalton Trans.* **2009**, 1267.
(13) Baranoff, E.; Fantacci, S.; De Angelis, F.; Zhang, X.; Scopelliti, R.; Grätzel, M.; Nazeeruddin, M. K. *Inorg. Chem.* **2011**, *50*, 451.
(14) Hofbeck, T.; Yersin, H. *Inorg. Chem.* **2010**, *49*, 9290.
(15) Orgel, L. E. *J. Chem. Soc.* **1961**, 3683.
(16) Nozaki, K. *J. Chin. Chem. Soc.* **2006**, *53*, 101.
(17) Jansson, E.; Minaev, B.; Schrader, S.; Agren, H. *Chem. Phys.* **2007**, *333*, 157.
(18) Harrigan, R. W.; Crosby, G. A. *J. Chem. Phys.* **1973**, *59*, 3468.
(19) Kober, E. M.; Meyer, T. J. *Inorg. Chem.* **1984**, *23*, 3877.
(20) Krausz, E.; Riesen, H. *Coord. Chem. Rev.* **1997**, *159*, 9.
(21) Riesen, H.; Wallace, L.; Krausz, E. *Mol. Phys.* **1996**, *87*, 1299.
(22) Obara, S.; Itabashi, M.; Okuda, F.; Tamaki, S.; Tanabe, Y.; Ishii, Y.; Nozaki, K.; Haga, M. A. *Inorg. Chem.* **2006**, *45*, 8907.
(23) Matsushita, T.; Asada, T.; Koseki, S. *J. Phys. Chem. C* **2007**, *111*, 6897.
(24) Tong, G. S. M.; Che, C. M. *Chem.—Eur. J.* **2009**, *15*, 7225.
(25) Minaev, B.; Agren, H.; De Angelis, F. *Chem. Phys.* **2009**, *358*, 245.
(26) De Angelis, F.; Belpassi, L.; Fantacci, S. *J. Mol. Struct.: THEOCHEM* **2009**, *914*, 74.
(27) Smith, A. R. G.; Riley, M. J.; Lo, S.-C.; Burn, P. L.; Gentle, I. R.; Powell, B. J. *Phys. Rev. B* **2011**, *83*, 041105(R).
(28) Smith, A. R. G.; Burn, P. L.; Powell, B. J. *ChemPhysChem* **2011**, *12*, 2429.
(29) Nozaki, K.; Takamori, K.; Nakatsugawa, Y.; Ohno, T. *Inorg. Chem.* **2006**, *45*, 6161.
(30) Li, J.; Djurovich, P. I.; Alleyne, B. D.; Yousufuddin, M.; Ho, N. N.; Thomas, J. C.; Peters, J. C.; Bau, R.; Thompson, M. E. *Inorg. Chem.* **2005**, *44*, 1713.
(31) Haneder, S.; Como, E. D.; Feldmann, J.; Lupton, J. M.; Lennartz, C.; Erk, P.; Fuchs, E.; Molt, O.; Münster, I.; Schildknecht, C.; Wagenblast, G. *Adv. Mater.* **2008**, *20*, 3325.
(32) Jacko, A. C.; McKenzie, R. H.; Powell, B. J. *J. Mater. Chem.* **2010**, *20*, 10301.
(33) Jacko, A. C.; Powell, B. J. *Chem. Phys. Lett.* **2011**, *508*, 22.
(34) Jacko, A. C.; Powell, B. J.; McKenzie, R. H. *J. Chem. Phys.* **2010**, *133*, 124314.
(35) Mason, W. R. *A Practical Guide to Magnetic Circular Dichroism Spectroscopy*; Wiley-Interscience: Hoboken, NJ, 2007.
(36) Stephens, P. J.; Devlin, F. J.; Chabalowski, C. F.; Frisch, M. J. *J. Phys. Chem.* **1994**, *98*, 11623.
(37) Becke, A. D. *J. Chem. Phys.* **1993**, *98*, 5648.
(38) Lee, C.; Yang, W.; Parr, R. G. *Phys. Rev. B* **1988**, *37*, 785.
(39) Schmidt, M. W.; Baldridge, K. K.; Boatz, J. A.; Elbert, S. T.; Gordon, M. S.; Jensen, J. H.; Koseki, S.; Matsunaga, N.; Nguyen, K. A.; Su, S.; Windus, T. L.; Dupuis, M.; John A. Montgomery, J. *J. Comput. Chem.* **1993**, *14*, 1347.
(40) Gordon, M. S.; Schmidt, M. W. In *Theory and Applications of Computational Chemistry: the first forty years*; Dykstra, C. E., Frenking, G., Kim, K. S., Scuseria, G. E., Eds.; Elsevier: Amsterdam, The Netherlands, 2005.
(41) Hay, P. J.; Wadt, W. R. *J. Chem. Phys.* **1985**, *82*, 299.
(42) Hehre, W. J.; Ditchfield, R.; Pople, J. A. *J. Chem. Phys.* **1972**, *56*, 2257.
(43) Ditchfield, R.; Hehre, W. J.; Pople, J. A. *J. Chem. Phys.* **1971**, *54*, 724.
(44) te Velde, G.; Bickelhaupt, F. M.; Baerends, E. J.; Guerra, C. F.; van Gisbergen, S. J. A.; Snijders, J. G.; Ziegler, T. *J. Comput. Chem.* **2001**, *22*, 931.
(45) Fonseca Guerra, C.; Snijders, J. G.; te Velde, G.; Baerends, E. J. *Theor. Chim. Acta* **1998**, *99*, 391.
(46) *ADF2009.01*; SCM, Theoretical Chemistry, Vrije Universiteit: Amsterdam, The Netherlands; http://www.scm.com/.
(47) van Lenthe, E.; Baerends, E. J.; Snijders, J. G. *J. Chem. Phys.* **1993**, *99*, 4597.
(48) van Lenthe, E.; Baerends, E. J.; Snijders, J. G. *J. Chem. Phys.* **1994**, *101*, 9783.
(49) Wang, F.; Ziegler, T. *J. Chem. Phys.* **2005**, *123*, 154102.
(50) Chong, D. P. *Mol. Phys.* **2005**, *103*, 749.
(51) Lenthe, E. V.; Baerends, E. J. *J. Comput. Chem.* **2003**, *24*, 1142.
(52) Hirshfeld, F. L. *Theor. Chim. Acta* **1977**, *44*, 129.
(53) Neese, F.; Petrenko, T.; Ganyushin, D.; Olbrich, G. *Coord. Chem. Rev.* **2007**, *251*, 288.
(54) Fouqueau, A.; Casida, M. E.; Daku, L. M. L.; Hauser, A.; Neese, F. *J. Chem. Phys.* **2005**, *122*, 044110.
(55) Fouqueau, A.; Mer, S.; Casida, M. E.; Daku, L. M. L.; Hauser, A.; Mineva, T.; Neese, F. *J. Chem. Phys.* **2004**, *120*, 9473.
(56) Finkenzeller, W. J.; Yersin, H. *Chem. Phys. Lett.* **2003**, *377*, 299.
(57) Finkenzeller, W. J.; Hofbeck, T.; Thompson, M. E.; Yersin, H. *Inorg. Chem.* **2007**, *46*, 5076.
(58) Rausch, A. F.; Thompson, M. E.; Yersin, H. *Inorg. Chem.* **2009**, *48*, 1928.
(59) Finkenzeller, W. J.; Thompson, M. E.; Yersin, H. *Chem. Phys. Lett.* **2007**, *444*, 273.

(60) Smith, A. R. G.; Riley, M. J.; Burn, P. L.; Gentle, I. R.; Powell, B. J.; Krausz, E.; Hall, J. (to be published).
(61) Knox, R. S. *Photochem. Photobiol.* **2003**, *77*, 492.
(62) Riesz, J. J.; Gilmore, J. B.; McKenzie, R. H.; Powell, B. J.; Pederson, M. R.; Meredith, P. *Phys. Rev. E* **2007**, *76*, 021915.
(63) Sajoto, T.; Djurovich, P. I.; Tamayo, A. B.; Oxgaard, J.; Goddard, W. A.; Thompson, M. E. *J. Am. Chem. Soc.* **2009**, *131*, 9813.
(64) Plischke, M.; Bergersen, B. *Equilibrium Statistical Physics*; World Scientific: Singapore, 2006.